Heliyon 9 (2023) e23107

Contents lists available at ScienceDirect

Heliyon

journal homepage: www.cell.com/heliyon

# Development of a highly concentrated collagen ink for the creation of a 3D printed meniscus

Alfredo Ronca [a], Ugo D'Amora [a,*], Elisa Capuana [a], Carla Zihlmann [b], Niklaus Stiefel [b], Girish Pattappa [c], Ruth Schewior [c], Denitsa Docheva [c,d], Peter Angele [c,e], Luigi Ambrosio [a]

[a] Institute of Polymers, Composites and Biomaterials, National Research Council, Naples, Italy
[b] Geistlich Pharma AG (Geistlich), Bahnhofstrasse 40, CH-6110 Wolhusen, Switzerland
[c] Experimental Trauma Surgery, Department of Trauma Surgery, University Regensburg Medical Centre, Regensburg, Germany
[d] Department of Musculoskeletal Tissue Regeneration, Orthopaedic Hospital König-Ludwig-Haus, University of Wurzburg, Germany
[e] Sporthopaedicum Regensburg, Hildegard von Bingen Strasse 1, 93053 Regensburg, Germany

ARTICLE INFO

*Keywords:*
Collagen
3D printing
Meniscus tissue engineering
Vascular and avascular regions

ABSTRACT

The most prevalent extracellular matrix (ECM) protein in the meniscus is collagen, which controls cell activity and aids in preserving the biological and structural integrity of the ECM. To create stable and high-precision 3D printed collagen scaffolds, ink formulations must possess good printability and cytocompatibility. This study aims to overlap the limitation in the 3D printing of pure collagen, and to develop a highly concentrated collagen ink for meniscus fabrication. The extrusion test revealed that 12.5 % collagen ink had the best combination of high collagen concentration and printability. The ink was specifically designed to have load-bearing capacity upon printing and characterized with respect to rheological and extrusion properties. Following printing of structures with different infill, a series of post-processing steps, including salt stabilization, pH shifting, washing, freeze-drying, crosslinking and sterilization were performed, and optimised to maintain the stability of the engineered construct. Mechanical testing highlighted a storage modulus of 70 kPa for the lower porous structure while swelling properties showed swelling ratio between 9 and 11 after 15 min of soaking. Moreover, human avascular and vascular meniscus cells cultured on the scaffolds deposited a meniscus-like matrix containing collagen I, II and glycosaminoglycans after 28 days of culture. Finally, as proof-of-concept, human size 3D printed meniscus scaffold were created.

## 1. Introduction

The menisci, which are two semilunar discs of fibrocartilaginous tissue, are essential for preserving knee biomechanics and homeostasis because they allow joint lubrification, proprioception, load transfer, stability, nourishment, and shock absorption [1,2]. After injury, meniscal tissue can suffer functional loss and permanent alterations lead to a high risk of osteoarthritis [3]. Usually, to avoid further damage and to let the tissue regenerate, meniscal tears are sutured if the defect is not very large, and the surrounding tissue allows for possible fixation, particularly if this is located in the vascular region. If the suture cannot be done, allograft

* Corresponding author.
*E-mail address:* ugo.damora@cnr.it (U. D'Amora).

https://doi.org/10.1016/j.heliyon.2023.e23107
Received 4 October 2023; Received in revised form 14 November 2023; Accepted 27 November 2023
Available online 1 December 2023

transplantation is a treatment option, although it has limitations such as mismatching, high costs and lack of readily available tissue sources [4].

Therefore, creating an engineered biomaterial construct that can imitate the physico-chemical and morphological characteristics of native tissue (i.e., mechanical stability, vascularity, pore size, and anisotropy) and ultimately stop the onset of osteoarthritis could result in better clinical outcomes [5]. Anatomically, the meniscus is constituted by an extremely hydrated matrix (72 % of water), with the remaining 28 % consisting of organic matter, namely cells and extracellular matrix (ECM). The predominant fibrillar component of the meniscus is collagen, and the quantity varies depending on the meniscus's region. The composition of the meniscus ECM is 75 % (dry weight) collagen with predominantly collagen I throughout the structure. Type I collagen predominates in the outer vascular zone (80 % dry weight), with fewer than 1 % of other collagen types (such as type II, III, IV, VI, and XVIII) present. Only two forms of collagen, types I (40 %) and II (60 %), make up the 70 % by dry weight of collagen in the inner avascular area, together with elastin, adhesion glycoproteins, and glycosaminoglycans (GAGs) [6]. Because of its distinctive fibrillar structure, collagen regulates cells' shape, adhesion, migration, and differentiation, preserving ECM's biological and structural integrity [6]. To date, even if there are different types of scaffolds under investigation [7,8], only a few products have been employed for meniscus treatment in current clinical application. It is worth citing: Actifit (Orteq, London, UK), made of polycaprolactone (PCL)/polyurethane (PU) and the NUsurface (Active Implants, LLC, Memphis, USA), composed of PU [9–11]. However, these products have different drawbacks, such as inadequate conformity to patient meniscus or knee morphology, instability under complicated loading conditions (such as compressive, tensional, and shear loads), poor blood supply infiltration, and the use of synthetic polymers [12]. Therefore, there is a clinical need to provide innovative products to save meniscal function in humans.

3D printing/bioprinting is gaining popularity in the development of innovative solutions for meniscal regeneration due to the ability to manufacture biodegradable meniscus scaffolds using hydrogel biomaterials [13,14]. 3D bioprinting creates 3D bio-engineered structures by accurately depositing appropriate inks (i.e., a combination of biomaterials, with or without cells and/or bioactive agents) in a preplanned way using computer-aided design (CAD) and additive manufacturing (AM) processes. Numerous hydrogels have been used to develop inks for 3D printing of meniscal replacement. Among them, hyaluronic acid, collagen, and alginate have found extensive application as acellular biomaterial scaffolds because of their bioactivity, mechanical characteristics, and material processability [15–17]. Hydrogels intrinsically have hydrophilic structures that allow them to retain substantial amounts of water or any aqueous biological fluid without dissolving, providing a naturally hydrated tissue-like environment [18,19]. At a biomolecular level, this swelling behaviour facilitates the diffusion of molecules and infiltration of cells [20]. To create stable and high-precision constructs, ink formulations must possess good printability and cytocompatibility. The printability of the material depends upon its rheological behaviour coupled with printing parameters that allow the deposition of materials in filament/strand form [21]. Specifically, the shape fidelity and the mechanical features of the final construct depend upon the composition and concentration of the ink. Collagen has been successfully employed in clinical practice for many years. Interestingly, 3D printed collagen scaffolds have been reported to be more feasible due to their tuneable mechanical properties and their similarities to the original tissue [5,22]. However, it has been demonstrated that the use of pure collagen, as an ink in low concentrations (usually, not more than 0.5 and rarely, 1 %) does not exhibit good rheological properties for creating 3D scaffolds, beyond 1–2 mm thickness and often leads to structural collapse [2,23]. To successfully manufacture a 3D printed human meniscus implant, a similar height to current products (e.g., Actifit is around 8 mm in height) is required [10]. Osidak et al. reported that the collagen concentration of a printed hydrogel did not negatively influence cell viability, whereas by increasing it, the compression modulus of the printed gels linearly increased [24,25]. It was shown by Diamantides et al. that raising the collagen inks' storage modulus prior to extrusion was the most effective method of enhancing printability [26]. In fact, there are few high-concentrated inks available, whereby their concentrations do not exceed 8 % (Viscoll Bioink) [25,27]. For instance, Lode et al. were able to optimize the printing of high-density collagen inks in a pH 4 swollen condition, with a dry matter concentration of no more than 4 % [28]. In particular, the authors showed that the collagen matrix can be easily and affordably shaped into a predetermined configuration using the plotting procedure without a temperature control or other components. The stabilization of the plotted structures was accomplished via freeze-drying and chemical crosslinking, similar to the construction of scaffolds by mould-casting. The resulting scaffolds were stable in cell culture conditions and possessed a high degree of shape and dimensional fidelity as well as a hierarchical porosity (macropores created by fibers deposition and an interconnected microporosity inside the strands due to the freeze-drying process). Through seeding of human mesenchymal stem cells (hMSCs), the scaffold's cytocompatibility and prospective utility for both hard and soft tissue engineering (TE) were proven [28].

Herein, the present work focused on the development and characterization of a high-concentrated collagen-based ink (higher than 10 %) to be used in 3D printing for meniscus tissue regeneration. Specifically, the idea attempted to create an ink entirely derived from collagen with high printability, shape fidelity and mechanical properties required for load-bearing tissues. Medical grade collagen was derived from a decellularized porcine tissue source. The ink was prepared at different collagen concentrations and the optimal concentration in terms of rheological properties and printability by 3D printing was tested. Following printing, a series of post-processing steps, including freeze-drying and crosslinking were performed, and optimised to maintain the dimensions and stability of the engineered construct. Finally, this study also performed *in vitro* tests on cell matrix deposition comparing human avascular and vascular meniscus cells to observe whether there were differences in their matrix deposition on the printed structures, mechanics, and biodegradation of the obtained structures to ensure sufficient feasibility and functionality of the scaffold. As a proof of concept, a human size meniscus scaffold was also produced by 3D printing to highlight the feasibility of the process.

## 2. Materials and methods

### 2.1. Preparation and characterization of collagen-based ink

A clinically used decellularized medical grade collagen for cartilage and bone regeneration was donated by Geistlich Pharma AG. Medical grade collagen, containing collagen type I and III, was milled using a 0.1 mm sieve. Inks with different collagen concentrations (10 %, 12.5 %, and 15 %) were prepared using phosphate buffer saline solution (PBS, Sigma Aldrich, IT). The ink was manually mixed for 1 min and tested at neutral pH. Later inks at 12.5 % were prepared as above and then the pH was adjusted to 3.5, by adding a small volume of phosphoric acid (Sigma Aldrich, IT), to obtain a smooth and homogeneous ink. The ink at 12.5 % collagen and pH 3.5 was also prepared by using a static mixer to induce more homogeneous pressure forces during ink extrusion for 3D printing process. After the static mixing step, the ink was transferred to a syringe, centrifugated at 2350×*g* for 3 min, to remove any remaining coarser air bubbles incorporated into the ink during mixing. Before printing/extruding, the ink was heated up to 30 °C for at least 10 min.

#### 2.1.1. Extrusion test

To evaluate printability of the ink, an extrusion test was performed using a uniaxial compression testing machine (Zwick & Roell Z2.5, Ulm, GE). The test was carried out on an ink-filled 10 mL plastic syringe equipped with a 0.61 mm inner diameter needle (Gauge 20) and an extrusion speed of 4 mm/s, at the needle tip, which was the common speed adopted from the 3D printing process. Smaller needles, for example, were insufficient to extrude such viscous inks while maintaining a suitable resolution of the finished prototype. In a preliminary test, different collagen concentrations were tested (10 %, 12.5 % and 15 %) to identify the most concentrated extrudable ink. The effect of pH and the mixing with the static mixer were compared, as previously decribed.

#### 2.1.2. Rheological characterization

The rheological tests were performed using an oscillation rheometer (Anton Paar, MCR301, Graz Austria) with a plate/plate geometry at 30 °C. Due to the size of the collagen fibers used in the ink, the distance between the plates was optimised and defined at 4 mm. First, an amplitude sweep with a subsequent relaxation-stress test was performed to simulate the viscoelastic properties of the ink in the syringe, prior to extrusion through the needle. The measurement was conducted at a shear deformation of $1 \times 10^{-5}$ to 1, angle velocity of 10 $s^{-1}$. The stress relaxation started with 8 s of shear deformation 1, which simulated the extrusion of the ink through the needle. Shear deformation was then dropped to 0.001 for the next 60 s to observe the recovery of the gel structure. In the amplitude sweep, both the elastic ($G'$) and viscus moduli ($G''$) at the end of the linear viscoelasticity range, the yield stress, and the shear strain at the point when the two moduli crossed were evaluated. Immediately following the relaxation test, the crossover of the two moduli after the decrease of the shear deformation is of great importance since this gives information on how fast the ink recovers to the paste-like structure after extrusion.

### 2.2. 3D printing of collagen ink and post-processing optimization

3D printing was performed by "Rokit Invivo 4D2" (Rokit Healthcare Inc., South Korea) with 1.80 firmware. The input print pattern was sliced using NewCreatorK 1.57.70. A 10 mL Luer-Lock glass syringe with an inner diameter of 15.5 mm was filled with the 12.5 % ink. The printing speed was set to 4 mm/s. The dispenser temperature was adjusted to 30 °C. Inner diameter needle size of 0.61 mm, a layer thickness of 0.4 mm, input flow of 110 % and infill densities of 40 % and 70 % were used to fabricate collagen structures with two different shapes: a block-like shape of $5 \times 5 \times 3$ $mm^3$ (width x length x height), and a cylindrical-like shape with 13 mm diameter and 3 mm height. According to the specific scaffold characterization, one of these forms was used.

After printing, prototypes followed a post-processing phase. First, they were incubated for 2 h in a 20 % w/w sodium chloride (NaCl, Sigma Aldrich, IT), followed by a 2 h incubation step in 20 mM PBS (pH 8.8). Samples were then freeze-dried with a freezing rate of 0.1 °C/min (Lyobeta 5 P S I Freeze dryer, Telstar, Barcelona, Spain). Dimensions to define shrinkage after freeze-drying were measured using a calliper. The NaCl content was monitored during the washing steps using a conductivity meter. Chemical cross-linking with 1-ethyl-3-(3-dimethylaminopropyl) carbodiimide hydrochloride/N-Hydroxysuccinimide (EDC and NHS, Sigma Aldrich, IT) was performed, as described elsewhere (Patent US2016166737A1). Finally, the scaffolds were sterilised by using an appropriate dose of X-ray, according to ISO 11137–1, in an industrial environment.

#### 2.2.1. Semi-sterile 3D printing and post-processing

Samples for endotoxin tests, as well as for biological characterization, were 3D printed and post-processed in semi-sterile conditions. To this aim, pyrogen free water and consumables were used. Moreover, the "Rokit Invivo 4D2" printer had high efficiency particle air filters, a laminar flow cover and ultraviolet sterilization lamp. All employed equipment was either single use, glass ware was intensively cleaned, and heat treated before use.

### 2.3. Scaffold characterization

All the analyses in the following sections were conducted on sterilised samples.

#### 2.3.1. Differential scanning calorimetry

For differential scanning calorimetry (DSC) analysis, sterilised samples were punched out, weighed, and transferred into 100 μL

aluminium crucibles and wetted with 40 μL PBS, pH 7.4. Before DSC analysis, the crucibles were closed and incubated for at least 2 h at room temperature.

#### 2.3.2. Collagen degradation kinetics

Sterilised samples were incubated at 1 mg/mL in 50 units/mL collagenase (Sigma Aldrich, IT) in 0.1 M tris buffer pH 3.7. During incubation at 37 °C, the detergent-compatible (DC) protein assay (Bio-Rad DC Protein Assay Kit, Biorad Laboratories, Munich, GE) was used to assess the protein concentration using bovine serum (BSA, Sigma Aldrich, IT) as standard, according to the manufacturer's protocol. Buffer with collagenase but no sample served as a negative control, whilst sterile Geistlich Bio-Gide served as a positive control.

#### 2.3.3. Morphological investigation

Scanning electron microscopy (SEM, FEI Quanta 200 FEG, USA) was used to observe the 3D additive manufactured scaffolds. Using an ion sputter, freeze-dried cylindrical scaffolds were coated with an ultrathin layer of Aurum/Palladium (Au/Pt) for sample preparation, and SEM imaging was performed.

#### 2.3.4. Mechanical characterization

The cylindrical scaffolds underwent dynamic mechanical analysis (DMA) using TA-Q800 (TA-Instrument, New Castle, DE, USA). The storage modulus (E') was measured at 0.5, 1.0, 5.0, and 10.0 Hz, where 1.0 Hz and 10 Hz simulated the normal and the limit of physiological stride frequency. In addition, a force track of 125 %, a preload of 0.001 N, and an amplitude of 100 μm in compression were chosen. The tests were performed in a closed chamber in a wet state, by using PBS at room temperature. The dehydration of the samples was not an issue because the measurement process only took a few minutes.

#### 2.3.5. Swelling behaviour

Final 3D cylindrical scaffolds were weighed ($w_0$) and left to swell in physiological conditions for up to 21 days (pH = 7.4, T = 37 °C) in 5 mL sterile Phenol red-free Dulbecco's Modified Eagle Medium-Low Glucose (DMEM-LG, Invitrogen, GE) supplied with antibiotics. The swollen hydrogels were removed at certain time periods and immediately tamponade to remove medium absorbed on the surface to evaluate their water retention capacity. Then, the weight was recorded ($w_t$), and the samples were placed back into the medium. Equation (1) was used to compute the swelling ratio (Q):

$$Q = (w_t\text{-}w_0)/w_0 \quad (1)$$

#### 2.3.6. Endotoxin test

The endotoxin level, expressed in endotoxin units (EU/sample), was quantified according to Ph. Eur. 5.1.10/2.6.14 Methode C, as well as USP <85> Photometric Quantitative Techniques, Turbidimetric Technique. Only depyrogenized materials were used for this test, whereby a defined amount of mass of the sample (300 mg) was added to *Limulus amebocyte* lysate reagent water (LAL - Pyroquant Diagnostik GmbH, GE). Supernatant was diluted with lysate. Photometrical measurement was conducted at 37 °C by using a Multiwell Infinite Plate Reader M200 (Tecan, GE), whereby the optical density (OD) value was assessed at 340 nm.

### 2.4. Biological characterization

#### 2.4.1. Meniscus cell isolation and cell seeding onto 3D printed scaffolds

Following informed consent from the patient and employing methods authorized by the regional ethics committee (University Hospital Regensburg; Ethical approval no.: Nr. 18-837-101), human meniscus tissue was obtained from patients (n = 3; mean age: 57 + 5) undergoing total knee arthroplasty (TKA) who had never previously sustained a meniscus injury.

Meniscus tissue was split into vascular (outer one third) and avascular (inner two thirds) regions. The tissue was then minced into smaller pieces and digested in two stages: first, for 45 min, in DMEM-LG + 5 % FBS (PAN-Biotech, GE) + 1 % penicillin-streptomycin (Sigma Aldrich, GE) with pronase (70 U/mL; Roche Diagnostics, CH) and then, for an additional overnight in collagenase type II (230 U/mL; Worthington) in the same conditions (37 °C). Isolated avascular and vascular meniscus cells were counted using a haemacytometer and then seeded at $5 \times 10^3$ cells/cm$^2$, cultured in DMEM +10 % FBS +1 % penicillin-streptomycin +5 ng/mL basic fibroblast growth factor (Peprotech, GE) + 1 ng/mL TGF-$\beta_1$ (R and D systems, UK) in a 37 °C/5 % $CO_2$ incubator. After five days, the media was changed for the first time. After that, it was changed twice a week until the cells reached 80 % confluence, at which point they were trypsinized and sent on to the next step. Sterile 70 % infill collagen scaffolds were selected for further biological investigation. Cells were cultured till passage 2 and then were trypsinized for cell seeding onto scaffolds. In brief, avascular, and vascular meniscus cells were trypsinized and counted using a haemacytometer. Then $1 \times 10^6$ meniscus cells/mL were injected into the scaffolds using a vacuum/perfusion system to enable even cell distribution [29]. Cell-seeded collagen scaffolds were incubated for 1 h and then cultured in 1 mL chondrogenic medium. The serum-free high-glucose DMEM contained: 100 nM dexamethasone (Sigma Aldrich, GE), 50 μg/mL ascorbic acid-2-phosphate (Sigma Aldrich, GE), 1 mM sodium pyruvate (Invitrogen, GE), 10 ng/mL transforming growth factor-β1 (TGF-β1, R&D systems), and 1 % ITS (PAN Biotech GmbH, GE). Three weekly media changes were made, and after 28 days, the data was gathered for study.

*2.4.2. Histological staining for cell-seeded collagen scaffolds*

Avascular and vascular meniscus cell-seeded collagen scaffolds (n = 3; 1 scaffold per donor) were embedded in Tissue-Tek (Sakura, NL) after being fixed in 4 % PBS buffered paraformaldehyde, washed in PBS, and incubated at room temperature in increasing sucrose concentrations (10–30 %). Cryosections (10 μm thick) were created using a cryostat (Leica CM1950; Leica, GE). Sulfated GAGs were observed by histochemical staining with DMMB (0.05 % 1,9-dimethylmethylene blue, 0.5 % ethanol, 0.2 % formic acid, 30 mM sodium formate, pH 3), as previously described [30].

Sections used for collagen I and II immunohistochemistry were stained as previously described and all steps were performed at room temperature [30]. In brief, sections were rehydrated and antigen retrieval was performed using 3 mg/mL pepsin (Sigma Aldrich, GE) in 1 × citric/phosphate McIlvaine buffer for 15 min. Following this, all sections were treated in blocking buffer (10 % goat serum in 1xPBS) for 1 h and stained with human type I collagen (mouse monoclonal antibody, 1:50; C256; Sigma Aldrich, GE) and human type II collagen (mouse monoclonal antibody, 1:200; CP18, Calbiochem, GE) in the same buffer and incubated overnight with gentle rocking. Biotinylated secondary antibody (goat anti-mouse IgG; 1:100) was detected with an HRP (Horse Radish Peroxidase)-labelled avidin–biotin complex and diaminobenzidine tetrahydrochloride hydrate as substrate (Vector, USA) [30].

*2.4.3. GAG assay and collagen I ELISA quantification for cell-seeded collagen scaffolds*

Following 28 days culture, a cell-seeded scaffold (n = 3, avascular and vascular donor) was collected and immediately frozen at −20 °C for quantification of GAG and collagen I within the scaffolds. Prior to digestion, the scaffold was split in half for each analysis. For GAG digestion, cell-seeded scaffold was minced into smaller pieces and then digested in 150 μg/mL papain in PBS, pH 6.0, containing 8 mM sodium EDTA, 6 mM L-cysteine (all Sigma Aldrich, GE). As previously mentioned, 1,9-dimethylene blue (DMMB) and Picogreen (Quant-iT dsDNA; Invitrogen, USA) assays were used to measure the amount of sulfated GAG and DNA [30].

Collagen I was extracted from the other half cell-seeded scaffolds via homogenization using a PreCellys homogenizer (Bertin Instruments, FR), then digested using 10 mg/mL pepsin in 0.05 M acetic acid, 0.5 M NaCl, pH 2.9 with continuous shaking at 4 °C for 48 h. Subsequent steps and ELISA were performed according to the manufacturer's protocol (Type I Collagen detection kit, Chondrex, USA; intra-assay reproducibility: 1.4–3.9 % and inter-reproducibility: 2–6.6 % for human collagen I range 0.16 μg/mL-2.5 μg/mL) and DNA content was measured as described above.

*2.4.4. Gene expression analysis from cell-seeded collagen scaffolds*

RNA was extracted from a cell-seeded scaffold for both avascular and vascular meniscus cells. Scaffold was snap frozen, minced into small pieces, QIAzol (Qiagen, GE) added and then homogenised using a PreCellys system homogenizer. RNA Solution was removed and isolated using the QIAzol method, then genomic DNA removed and RNA purified via RNeasy Mini kit (Qiagen, GE). All steps were completed according to the manufacturers' instructions. 500 ng of total RNA were reverse transcribed using the Transcriptor first strand kit (Roche, GE) after the amount of RNA was measured. The Brilliant SYBR Green QPCR mix (Stratagene, USA) was used to perform qPCR reactions for chondrogenic genes (Table 1), and the Biorad CFX96 equipment (Biorad Laboratories, GE) was used to measure the results. Proteasome subunit beta type-4 (PSMB4) was utilized as a housekeeping gene during the data analysis utilizing the ΔΔCt method. Results were reported as fold change relative to monolayer meniscus cells (P2).

*2.4.5. In vitro biomechanical analysis*

The seeded and acellular scaffolds were mechanically analysed by DMA after 28 days of incubation, to understand the effect of collagen deposition and matrix degradation on scaffold mechanical properties. Samples after 28 days of culture underwent multi-frequency compression test, as described in paragraph 2.3.4. The mechanical properties of the cell seeded scaffolds were then compared with E' modulus of the acellular scaffold, after 28 days of culture in medium, to understand the mechanical role of collagen deposition and matrix degradation of the proposed scaffold.

*2.5. 3D printing of anatomically shaped human meniscus scaffold*

To assess the feasibility of a clinically relevant printing process, a human meniscus, with its complex anatomically shaped structure, was printed based on generic models. A simplified shape of the human medial meniscus was selected to be suitable for 3D printing application. The 3D meniscus model was converted to standard tessellation format (.stl) by Rhinoceros 4.0 (Robert McNeel & Associates, USA) and sliced using Rokit software for the 3D printing process. The collagen ink (12.5 %) was 3D printed by "Rokit Invivo 4D2" using the same printing parameters reported above, a grid pattern and 70 % of infill.

**Table 1**
Gene and primer sequences designed for evaluating cell-seeded 3D printed collagen scaffolds [31].

| Gene | Sequence (Forward) | Sequence (Reverse) | NCBI Accession Number |
|---|---|---|---|
| *PSMB4* | GCTTAGCACTGGCTGCTTCT | GGACATGCTTGGTGTAGCCT | NM_002796.3 |
| *SOX9* | ACACACAGCTCACTCGACCTTG | AGGGAATTCTGGTTGGTCCTCT | NM_000346.4 |
| *COL1A1* | ACGTCCTGGTGAAGTTGGTC | ACCAGGGAAGCCTCTCTCTC | NM_000088.4 |
| *COL2A1* | GGGCAATAGCAGGTTCACGTA | TGTTTCGTGCAGCCATCCT | NM_033150.3 |
| *ACAN* | GGCACTTCAGTTGCAGAAGG | CTATACCCCAGTGGGCACAT | NM_001135.4 |

### 2.6. Statistical analysis

For all statistical analyses, Graphpad Prism v7 (GraphPad, USA) was used. Using the Shapiro-Wilk test, the normal distribution of the data was examined. An unpaired *t*-test was used to compare the GAG and collagen I content of vascular and avascular meniscus cells, with a significance threshold of $p < 0.05$. A Mann-Whitney test was used to analyze the gene expression data, which was expressed as a fold change in comparison to the meniscus cells on day 0. The significance level was established at $p < 0.05$.

## 3. Results and discussions

### 3.1. Collagen ink characterization

Solubilized collagen is a low-viscosity material and thus its concentration within 3D printing inks affects its success. To improve printability and mechanical strength, the addition of other biomaterials [32,33] or the increase of concentration has been widely reported [26,28,34]. In the present study, single-component, high-density (from 10 % to 15 %) collagen inks were tested to create an accurate, large-scale 3D structure, without a supporting material during printing and *in situ* crosslinking. To assess printing ink homogeneity, they were directly tested in a 3D printing setting. Specifically, the extrusion force measurement was carried out using the same printing conditions (*i.e.,* speed, needle size, temperature) and placing the ink inside the same syringes. The extrusion distances imposed on the syringes also mimicked those of real printing. Therefore, the validity of the obtained results is certainly enhanced since the extrusion conditions closely matched those during 3D printing. Fig. 1a shows the results of extrusion force measurements for inks with different collagen concentrations, all at pH 7. Inks at pH 7 showed an unsteady extrusion of material resulting in fluctuating extrusion forces that are not suitable for 3D printing. Particularly, at 15 % collagen, the extrusion forces were higher than for inks at 10 and 12.5 %. Since we aimed for high shape fidelity, a more viscous ink was preferred. Therefore, the following experiments were made with inks containing 12.5 % collagen. To obtain a steady extrusion, the pH was lowered to pH 3.5 and again tested at a collagen concentration of 12.5 %. In comparison to pH 7, extrusion forces at pH 3.5 were steady (Fig. 1b) and could be smoothed by applying a

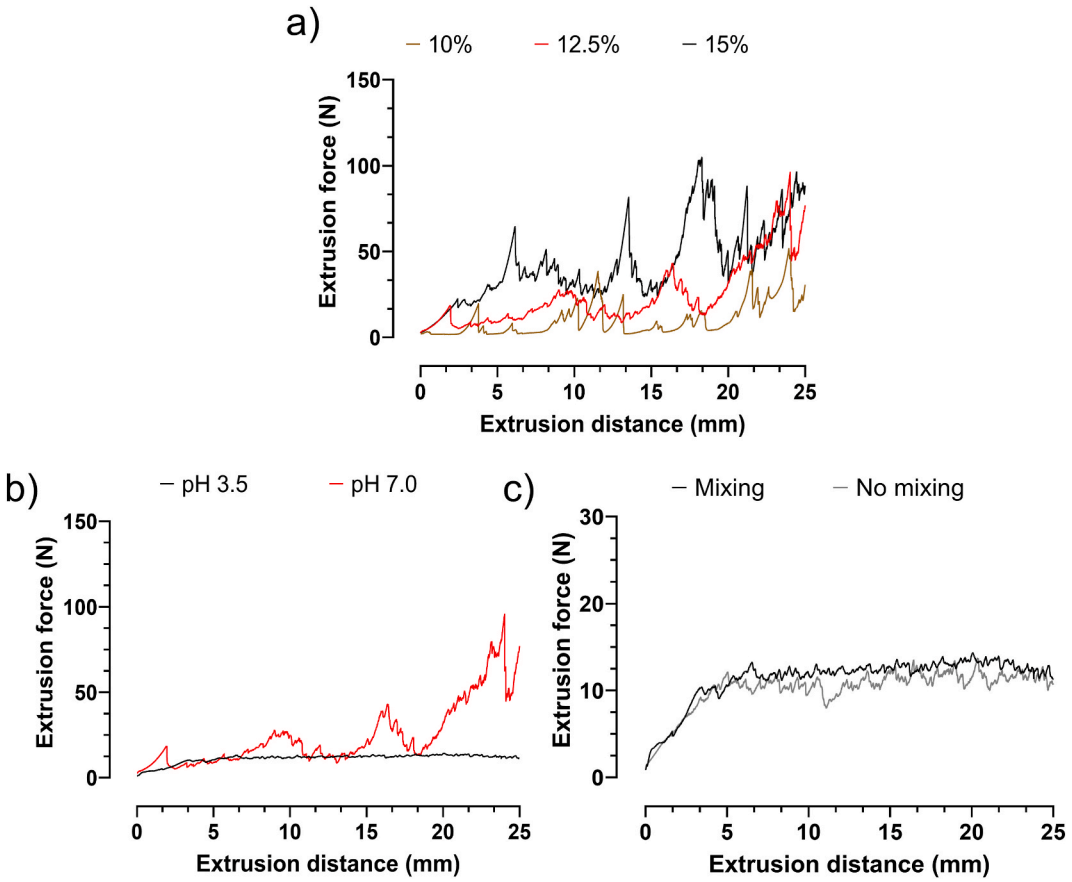


**Fig. 1.** a) Results from extrusion tests performed on inks with 10 %, 12.5 % and 15 % collagen at pH 7.0. Optimization and characterization of the ink formulation through different process steps, by: b) lowering the pH; c) a static mixing step. The black curve is the final ink formulation at a pH of 3.5, after static mixing.

static mixing step prior to 3D printing (Fig. 1c). Indeed, the collagen fibers, whose isoelectric point is around pH 7, swell when the pH of the slurry is below 4.5 and higher than 11. When the collagen fibers have an adequate positive or negative charge, the water creates a hydration coat around the fibers and the slurry appears to be homogeneous [28]. Conversely, the neutral pH displayed uneven dispensing and partial needle obstructions due to precipitated collagen clots that ultimately stopped the deposition of homogenous strands. Considering that the main goal was to employ the most concentrated printable ink, 12.5 % at pH 3.5 was selected for the proposed applications. Indeed, the ink with 12.5 % collagen at pH 3.5 was homogeneously extrudable and could maintain its shape after printing.

Fig. 1b and c shows the optimization process for the 12.5 % ink, through different steps, of pH modification and mixing, respectively. Indeed, the pH adjustment from 7 to 3.5 resulted in a lower fluctuation in extrusion force, indicating a higher homogeneity within the solution during flow, as described by others [35]. For instance, the positive effect of mixing on ink homogeneity during printing was also reported by Choen et al., who observed a reduction of up to 82 % in mechanical noise by increasing mixing cycles from 8 to 128 [36]. Furthermore, the optimised formulation showed an average extrusion force of 12.7 ± 0.2 N for an extrusion distance of 10–30 mm. This result is in line with the low range of extrusion force required to allow easy extrusion during printing, as shown for other materials [37,38].

The rheological characterization was performed by amplitude sweep to get information about the paste-like and fluid-like behaviours of the ink at low deformation, simulating the ink in the syringe, before extrusion, and at high deformation, simulating extrusion from the syringe (Fig. 2a). Particularly, the amplitude sweep was carried out to measure G′ and G″ at low strains, where the ink behaves as a gel and at higher strains where it acts as a fluid. Then, a subsequent relaxation test was carried out to study the recovery after extrusion, thus imposing a high deformation followed by a low deformation. This information was relevant since the ink must be printable and, once extruded, should be able to retain its shape and not collapse under the pressure of multiple filaments until post-processing (Fig. 2b).

As a result of amplitude sweep, at low shear deformation, the material was still in the pasty state. Then, as the deformation increased, there was a decrease in G′ and an increase in G″ until the two curves overlapped (Fig. 2a), so the behaviour of the ink changed from paste-like to fluid, as required for printing [39].

Fig. 2b shows the curves of the relaxation test that was performed to simulate ink recovery after printing into filaments deposited on the printing bed. The shear deformation was equal to 1 during the first 8 s, then instantaneously dropped to 0.001. As described in Fig. 2b, the overlapping of the two curves highlighted that the ink reversibly recovered and showed paste-like behaviour. In particular, G′ and G″ moduli crossed after 12 s, four seconds after the shear deformation was decreased to 0.001. This means that the recovery time, which is related to the changed behaviour from liquid to pasty was 4.1 ± 0.3 s. The recovery time was short enough to avoid fibres coalescence and reduced shape fidelity as described by Cooke et al. [40]. The shear deformation and the yield stress (y), corresponding to the values where G′ and G″ intersect were: 0.22 ± 0.008 and 1.3 ± 0.4 kPa, respectively. Meanwhile, G′ and G″ were: 5.1 ± 1.4 kPa and 0.65 ± 0.16 kPa. Inks with similar rheological properties demonstrated excellent shape fidelity filament formation [37]. In addition, inks with such properties prevented layer collapse, resulting in multilayer constructs with high layer height and good stacking quality [41]. Therefore, it was expected a similar behaviour with the ink under investigation.

### 3.2. 3D printing of scaffolds and post-processing

Scaffolds were successfully produced by 3D printing (Fig. S1 a,d). After 3D printing and post-processing, which includes stabilization using NaCl solution, washing, crosslinking, freeze-drying and sterilization, the resulting scaffolds should meet specifc requirements. In particular, the dimension of the samples should be preserved. To make the scaffold biocompatible, the pH should be

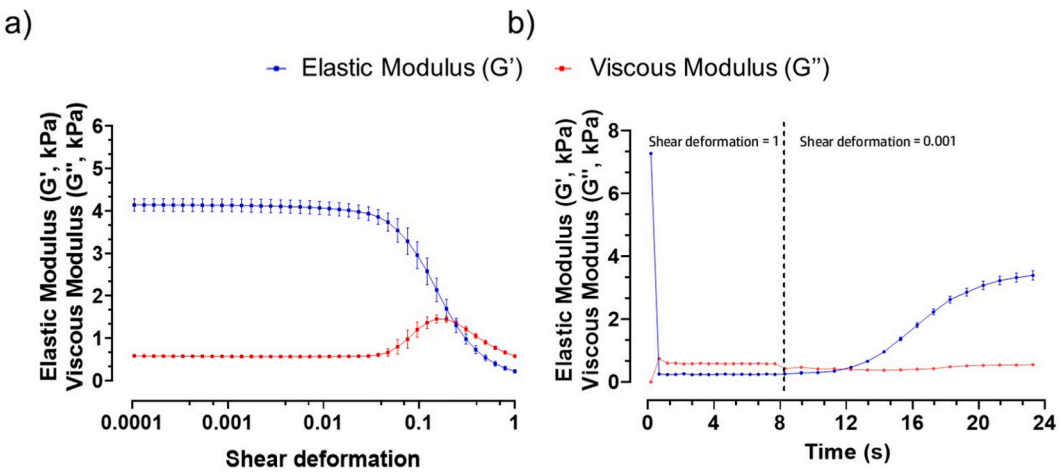


**Fig. 2.** Rheological properties obtained for the ink from: a) amplitude sweep, simulating the deformation of the ink during 3D printing; b) relaxation test. (Data represent mean ± standard deviation (S.D.); n = 6).

shifted towards a neutral pH, and the used NaCl during stabilization step should be removed to allow long-term storage at room temperature, the scaffold is preferred to be dry. Crosslinking degree needed to balance the mechanical stability of the scaffolds, whilst maintaining good biocompatibility. In addition, suitable sterilization parameters were also identified. To this aim, after 3D printing, NaCl was used to preserve the dimension through precipitation of the collagen. The resulting shrinkage was in the range of 1–5 %. No substantial shrinkage or swelling of the collagen scaffold occurred, and the 3D printed geometry remained intact as shown in Fig. S1 (b, e). Finally, after overnight incubation, the pH was high enough to fit in the target range of 6.5 and 8.5. The NaCl excess was partially removed during the described pH shift, as well as during further washing steps. The collagen was chemically crosslinked by the zero-length crosslinker EDC/NHS which forms amid bonds. These created amid bonds between the collagen fibers provide the structure mechanical strength and proteolytic resistance [42]. Samples were equilibrated at a defined air humidity of 55 % and 22 °C, then X-ray sterilised at 25–33 kGy. Even after the crosslinking, lyophilization and sterilization steps the scaffolds preserved the geometry and pores shape as shown in Fig. S1 (c, f) [43].

### 3.3. Scaffold characterization

#### 3.3.1. Differential scanning calorimetry

In the present work, results from DSC allowed obtaining the onset temperature of protein denaturation ($T_d$) (Fig. 3a). The onset temperature of protein denaturation of the sterilised 40 % infill scaffolds was 46.9 ± 1.0 °C, whereas the sterilised 70 % infill scaffold had the onset at 46.6 ± 0.3 °C. $T_d$ correlates with the crosslinking degree: slightly crosslinked materials ($T_d$ < 65 °C), moderately crosslinked materials ($T_d$ 65–70 °C), and heavily crosslinked ($T_d$ > 70 °C) [43,44]. The biocompatibility of collagen materials strongly depends upon their crosslinking degree [44]. According to Delgado et al. the scaffolds were classified as slightly crosslinked collagen networks and therefore good biocompatibility was expected [44]. It is worth noting that higher crosslinking degrees may lead to a higher mechanical strength, but as also widely reported, they may be also associated with macrophage response and polarisation. It would further correlate with reduced cell infiltration and increased proinflammatory cytokine expression [43,44].

#### 3.3.2. Collagen degradation kinetics

The collagen degradation kinetics was measured to address the degradability of both scaffolds (Fig. 3b and c). Between minute 10 and 30, the sterilised 40 % infill scaffold, as well as the sterilised 70 % infill scaffold, degraded in a linear slope. In the 40 % and 70 % infill scaffold, a slope of 410 ± 50 μg $mL^{-1}h^{-1}$ and 389 ± 79 μg $mL^{-1}$ $h^{-1}$, respectively were calculated. The 40 % and 70 % scaffolds degraded with the same speed. Both scaffolds degraded slower than the positive control (Chondro-Gide).

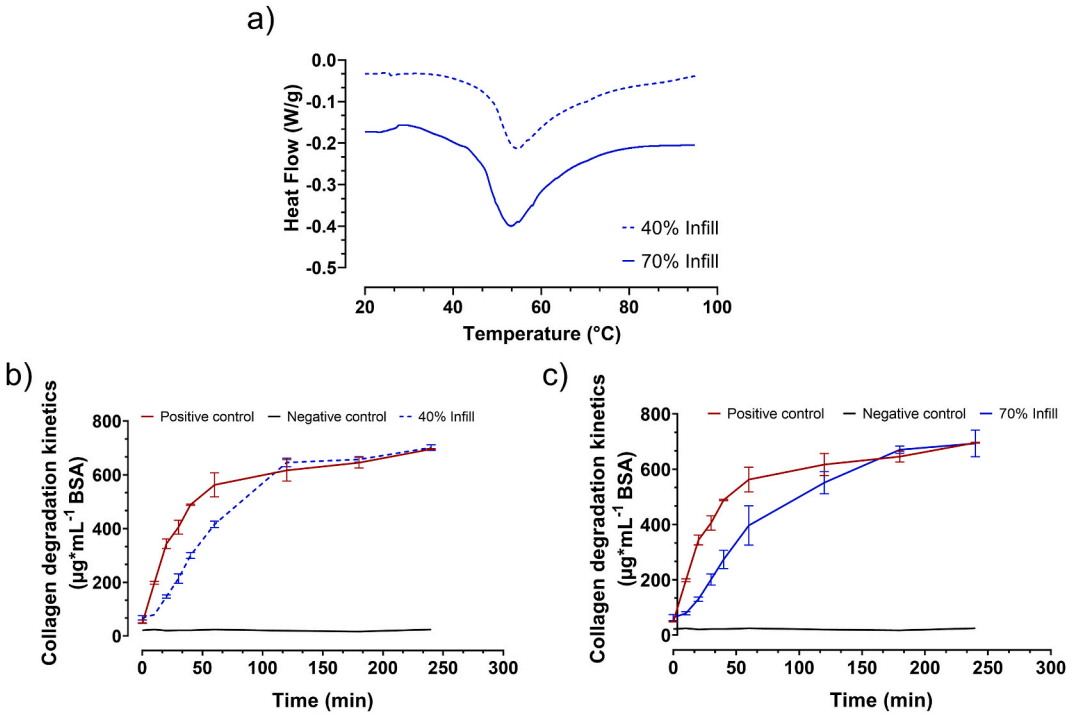


**Fig. 3.** DSC curves for scaffold with a) 40 % and 70 % Infill. Degradation kinetic of the collagen scaffold with (b) 40 % and (c) 70 % Infill. (Data represent mean ± S.D.; n = 6).

### 3.3.3. Morphological investigation

Collagen scaffolds maintained their 3D porous structure after printing and lyophilization, exhibiting a good shape fidelity of the printed macropores, as shown in Fig. 4. The fabricated collagen scaffolds resulted in interconnected micropores and macropores generated by the lyophilization process and 3D printing, respectively. When comparing the structures printed with the two infills, their micropores had similar average size, whereas the macropores were slightly larger in the lower-filled printed matrix. Specifically, the 40 % infill (Fig. 4 a-c) and 70 % infill (Fig. 4 *d*-f) scaffolds had regular macropores with a mean length of ~2 mm and ~900 μm after lyophilization, respectively.

The dense, interconnected structure of micropores had diameters in the range of 1–10 μm, whereas the filaments had an average size of 300 μm. It is worth noting that the scaffolds' morphology was assessed in dry conditions, it is expected that in physiological conditions, the pores are smaller, due to the slight swelling of the structure. Furthermore, following the implantation of the collagen scaffold, initial degradation activity is expected to start that also enlarges the pores over time. For meniscal tissue, it was reported that scaffolds with pore size between 200 and 500 μm promoted the maintenance of cell morphology, proliferation and ECM production [44–46]. Hence, the scaffolds produced in this work were suitable for meniscus repair because their average fibre size was within the range required for this regenerative purpose.

### 3.3.4. Mechanical characterization

DMA was used to characterise the mechanical behaviour of collagen scaffolds in the equilibrium swelling state. This condition was implemented because it has been shown that the mechanical response of collagen strongly depends on the hydration level [47,48].

Fig. 5a provides the DMA results of the collagen scaffold at 40 % and 70 % infill. Over the entire frequency range, E′ of the 70 % infill scaffold was higher than that of 40 % infill scaffold. An increase of E′ was detected with increasing the frequency in the analysed range (0.5 and 10 Hz). This increase was slight in the case of the scaffold with 40 % infill, marked in the other group. Smaller macropores significantly increased the E′ values, *i.e.,* the structure stiffness. For example, at the highest frequency investigated, the E′ value for the scaffold with 70 % infill was more than 70 kPa, almost a 5-fold increase over the structure with the lower infill. This result is in line with the findings of other authors, indicating an increase in stiffness when the porosity decreases [49,50]. The measured E′ moduli of the two scaffolds are comparable with the native menisci of the human knee, whose E' varies from 40 to 90 kPa depending upon the position and deformation undergone [51]. Furthermore, the results showed that the mechanical features of the scaffold produced by this strategy, can be controlled to closely match the stiffness of the native tissue by varying the macroscopic porosity of the printed collagen scaffold.

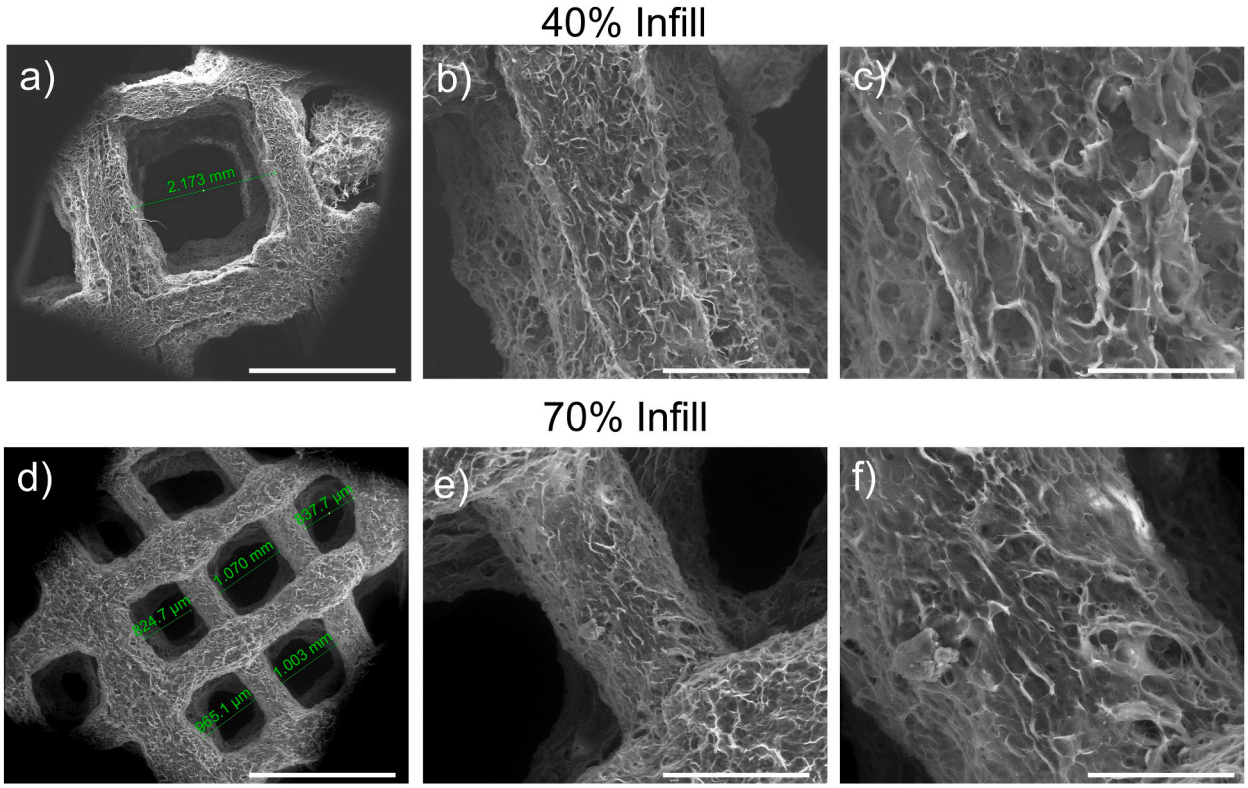


**Fig. 4.** SEM images of collagen-based scaffolds: (a, b, c) 40 % Infill; (d, e, f) 70 % Infill. Scale bars from left to right: 2 mm, 500 μm, 200 μm.

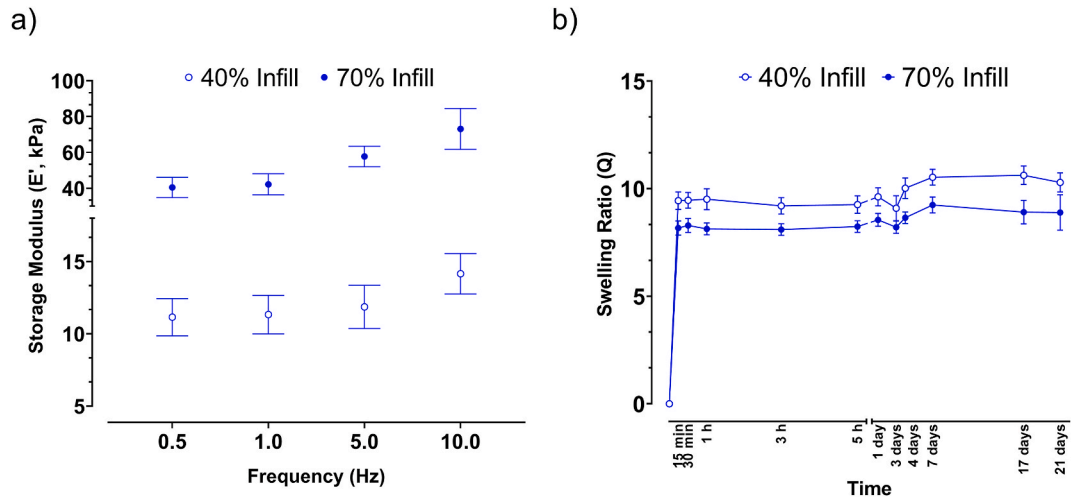


**Fig. 5.** a) Results from DMA tests performed on collagen-based scaffolds with two different infill percentages during printing (Data represent mean ± S.D.; n = 6). b) Swelling ratio of scaffold printed with 40 % and 70 % infill over 21 days. Both scaffold groups rapidly reached their swelling equilibrium, with no significant temporal effects after 21 days. (Data represent mean ± S.D.; n = 6).

### *3.3.5. Swelling behaviour*

The swelling ratio as a function of time for the two groups of scaffolds (*i.e.*, with 40 % and 70 % infill) is plotted in Fig. 5b. Both structures rapidly swelled, reaching an equilibrium swelling ratio value within 15 min. The scaffolds with lower infill and higher macroscopic porosity (40 % of infill), absorbed slightly more culture medium than the other, suggesting a mild increase in hydrophilic behaviour due to larger void spaces at the macroporous level. Structures at 40 % infill balanced at ~ 11 as swelling ratio, whilst those at 70 %, balanced at ~ 9. These data are in agreement with other works on hydrogels that found an increase in swelling ratio with increasing pore size [52]. Overall, collagen scaffolds were found to swell readily in culture medium due to many ionizable groups in the chain of collagen molecules, such as –NH groups and –COOH groups [53]. No significant time effects were observed for the scaffolds for both groups after 21 days of the swelling test.

### *3.3.6. Endotoxin test*

The preservation of clean conditions during the manufacturing process and the post-processing was another important consideration for the realization of the device. Endotoxin, commonly known as lipopolysaccharide (LPS), is found in Gram-negative bacteria's outer membrane. Biomedical materials must be as free or containing only low values of endotoxin because when endotoxin invades the body can cause fever, shock and even death [54]. In the present work, even though there was no obvious contamination, a quantification of endotoxins was conducted to see if it would be appropriate for future *in vivo* studies. Indeed, if not properly managed, endotoxin concentrations inside hydrogels can vary significantly [55]. In the present work, the results from endotoxin test showed values lower than 2.1 EU/device for all tested samples (n = 10) which were below the limit for medical devices equal or less of 20 EU/device [56].

## *3.4. Biological characterization*

Regarding the biological characterization, samples with 70 % infill were selected because morphological and mechanical properties were best balanced. Meniscus cells derived from avascular and vascular region were found to upregulate the cartilage-related transcription factor, SOX9 and matrix genes, ACAN, COL2A1 and COL1A1 upon culture within the 3D printed collagen scaffolds after 28 days in culture (Fig. 6a). Analysis of GAG content within the scaffolds showed that there was no significant difference in GAG content between avascular and vascular meniscus cells and this was further illustrated with metachromasia staining of both scaffold group ($p > 0.05$; Fig. 6b). Collagen I staining was observed in the surrounding scaffold with clear pores within the structure (Fig. 6c). However, cell-seeded scaffold showed matrix deposition within the structure with a more homogeneous staining throughout the scaffold with vascular cells tending to produce more collagen I, although there was no significant difference ($p > 0.05$; Fig. 6c). In contrast, there was no collagen II staining in the cell-free collagen scaffolds, whilst cell-seeded scaffolds showed collagen II deposition, although this was lower compared to collagen I staining (Fig. 6d). The gene expression, GAG, and collagen I data show no significant differences between the regions in the collagen scaffolds. This is contrary to the known differences between the regions in the native meniscus [57,58]. The reasons for the no specific differences between regions could be related to the meniscus origin from patients undergoing total knee arthroplasty and there is some level of osteoarthritis within the tissue, leading to similar matrix deposition between the zones. Furthermore, there has been evidence for no differences in matrix gene expression between regions [59]. Additionally, recent evidence has suggested that rather than two meniscus zones, there is a middle or transition between the avascular and vascular zone that is partially vascularised [60]. As the isolated avascular meniscus cells contained this region, this is also likely to

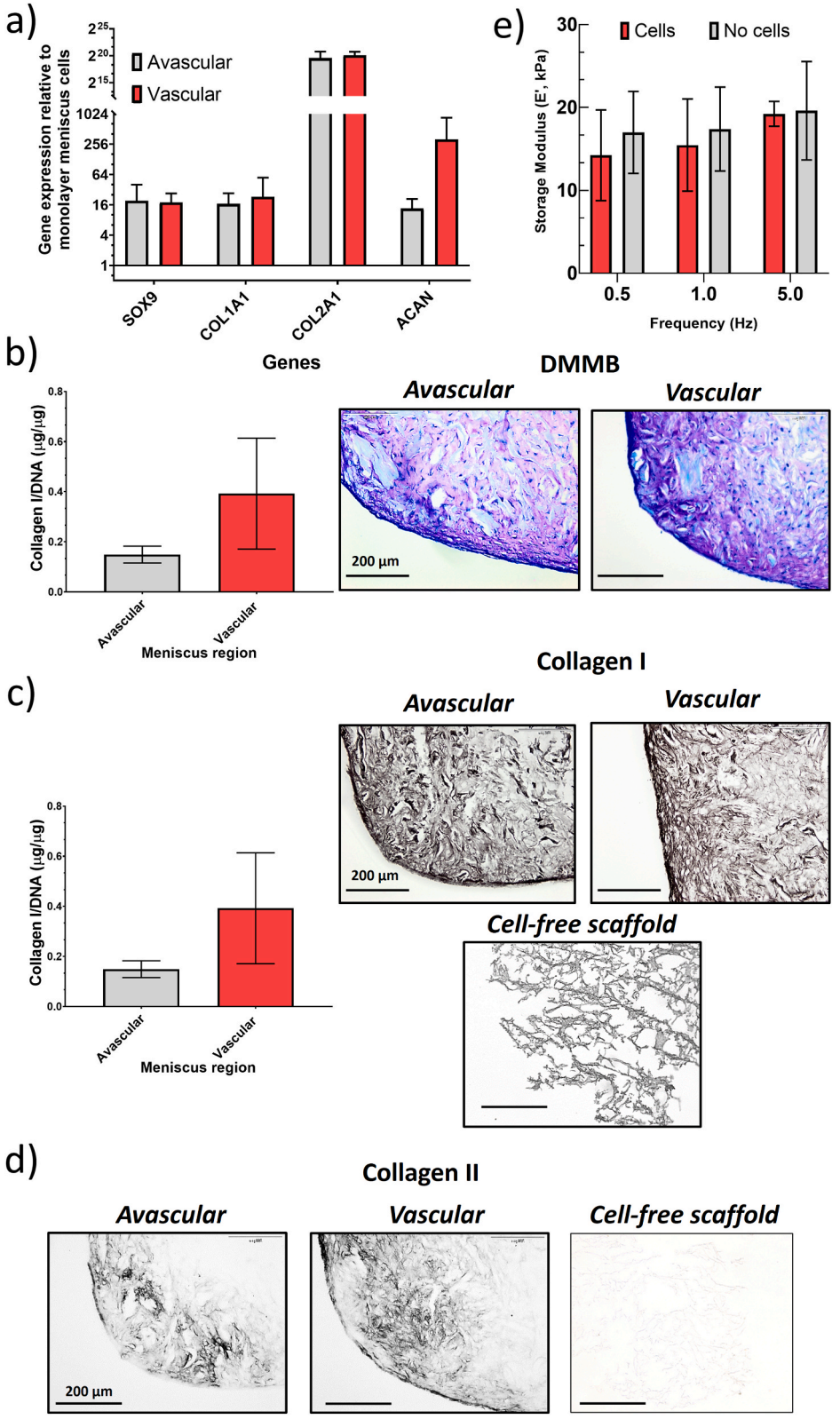


*(caption on next page)*

**Fig. 6.** a) Gene expression analysis of meniscus matrix genes (ACAN, COL1A1, COL2A1) and SOX9 transcription factor for avascular and vascular meniscus cells cultured on 3D printed scaffolds (70 % infill). Data represent fold change in avascular and vascular meniscus cells seeded within the collagen scaffolds relative to corresponding monolayer meniscus cells for each donor (Data represent mean ± S.D.; n = 3). b) GAG and representative DMMB histological staining c) collagen I content of meniscus cells within 3D printed collagen scaffolds and representative collagen I histological staining (Data represent mean ± S.D.; n = 3; scale bar = 200 μm). d) collagen II histological staining for meniscus cells cultured on 3D printed scaffolds. (Scale bar: 200 μm). e) Biomechanical testing results, Values of E′ are shown separately and compared for samples seeded with cells and blank constructs as a function of the testing frequency. (Data represent mean ± S.D.; n = 6).

reduce difference between regions. Environmental stimuli can help to increase matrix deposition by meniscus cells and potentially find underlying differences between regions. In this instance, use of hypoxic culture (2–5% oxygen) or mechanical stimulation that mimic the native environment of the knee could help to increase matrix deposition and also uncover more discernible differences between regions [31,61,62].

### *3.4.1. In vitro biomechanical analysis*

Results showed no significant difference in E' between the cells-free scaffolds and the cell-seeded scaffolds cultured for up to 28 days (Fig. 6e). Indeed, the greater stiffness of hydrogel fibres could suppress cell spreading due to a lower ability of the cells to elongate [63]. Therefore, cells remodelled the collagen matrix by proteolytically degrading the collagen matrix and therefore creating more pores. Overall, this testing method allows the comparative evaluation of scaffold seeded with cells and scaffolds with no cells with respect to their mechanical properties depending upon ECM microstructure [64].

## *3.5. 3D printing of anatomically shaped meniscus*

Using the high-concentration ink, meniscus scaffolds were successfully prototyped as a proof of concept without the need for a sacrificial material or a supporting thermoplastic frame. The printing process was accomplished without the use of intermediate chemical crosslinking procedures by adding successive layers in small incremental steps. Collagen is typically employed either alone or in combination with other materials to enhance mechanical and biological properties but many of these research studies focus on the printing of 3D objects such as block-shaped or cylinders. Only few papers have recently showed the ability to print more complicated, hollow objects [65,66]. Herein, the 3D printed meniscus scaffold in human size, as represented by the CAD model (Fig. 7a–c), preserved high shape fidelity, with its size matching the dimensions of the CAD. Furthermore, the scaffold was stable over time in PBS (Fig. 7d) and after lyophilization (Fig. 7e).

## 4. Conclusions

Meniscus regeneration remains a major challenge in clinical treatment due to its poor regenerative ability and structural complexity. A promising approach for patient-specific therapy is using 3D printed scaffolds. A suitable scaffold or implant should have an inner pore structure that allows for optimal mechanical stability, cell ingrowth, and vascularization, as well as an exterior form that

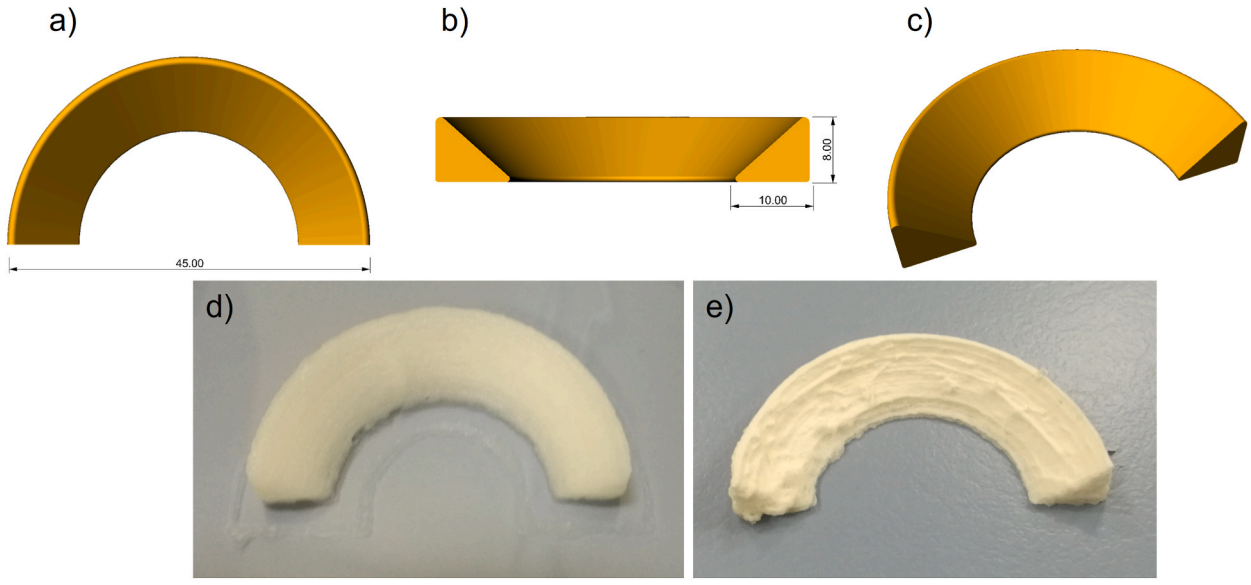


**Fig. 7.** 3D printing of meniscus scaffolds. a, b, c) CAD models of a human size meniscus. d) 3D printed structure after NaCl stabilization/pH shifting and washing. e) meniscus prototype after lyophilization.

correctly fits the defect. In this scenario, AM techniques and in particular 3D printing/bioprinting, have gained great attention for the manufacture of customized TE constructs by using a wide range of biomaterials. Among them, naturally derived materials have become more popular because of their capacity to replicate the ECM environment and promote cell adhesion, differentiation, and proliferation. Collagen, the most prevalent bioactive fibrous protein in the ECM, has been widely employed as biomaterial [28]. However, in literature only two strategies have been reported. The first one involves the printing of low concentrated ink that is unable to create 3D structures beyond 1–2 mm thickness while the second one, usually indicated as an indirect method, concerns the casting of the collagen ink in a sacrificial negative mould [67,68].

In the present work, to overlap the actual limitation in the 3D printing of pure collagen, the development of highly concentrated ink (12.5 %) as an ink for meniscus implant fabrication has been reported. The extrusion test revealed that 12.5 % ink had the best combination of a high collagen concentration and printability. Moreover, lowering the pH of the ink to acidic conditions (pH = 3.5) allowed a more homogeneous extrusion. Relaxation test highlighted that the ink had a short recovery time of about 4 s, allowing the creation of constructs with complex structure and maintaining the predesigned shape, without using any moulding or chemical/photo-crosslinking. Porous scaffolds with two different infills (40 % and 70 %) exhibited a good shape fidelity of the printed macropores and the presence of a microporosity, obtained by freeze-drying process. Mechanical analysis highlighted higher mechanical properties for the scaffolds with 70 % of infill, with a E′ higher than 70 kPa, almost a 5-fold increase over the structure with the lower infill. Based on the highest mechanical properties and the lowest swelling ratio, the *in vitro* characterization was performed only on the 70 % infill samples. Human avascular and vascular cells cultured on these 3D printed scaffolds deposited a meniscus-like matrix containing collagen I, II and GAGs after 28 days of culture, indicating that functional matrix is deposited on these scaffolds. Furthermore, biomechanical testing comparing cell-seeded and cell-free collagen scaffolds showed no significant difference in E' modulus. Future studies would seek to use environmental stimuli (e.g., hypoxia or mechanical stimulation) to see how these cell-scaffold would perform under *in situ* conditions and see if there are changes between meniscus cell regions and an increase in mechanical properties. Finally, as proof of concept, a human size meniscus scaffold was realized to demonstrate the possibility to print complex geometries without the use of supporting materials.

## Data availability

Data will be made available on request.

## CRediT authorship contribution statement

**Alfredo Ronca:** Writing – review & editing, Writing – original draft, Visualization, Validation, Supervision, Methodology, Investigation, Data curation, Conceptualization. **Ugo D'Amora:** Writing – review & editing, Writing – original draft, Visualization, Validation, Supervision, Methodology, Investigation, Data curation, Conceptualization. **Elisa Capuana:** Writing – review & editing, Writing – original draft, Visualization, Validation, Software, Methodology, Investigation, Data curation. **Carla Zihlmann:** Writing – review & editing, Validation, Methodology, Investigation. **Niklaus Stiefel:** Writing – review & editing, Validation, Methodology, Investigation, Conceptualization. **Girish Pattappa:** Writing – review & editing, Validation, Methodology, Investigation, Conceptualization. **Ruth Schewior:** Writing – review & editing, Validation, Methodology, Data curation. **Denitsa Docheva:** Writing – review & editing, Validation, Methodology. **Peter Angele:** Writing – review & editing, Supervision, Resources, Funding acquisition. **Luigi Ambrosio:** Writing – review & editing, Supervision, Resources, Project administration, Funding acquisition.

## Declaration of competing interest

The authors declare the following financial interests/personal relationships which may be considered as potential competing interests:Luigi Ambrosio reports financial support was provided by EU (European) Framework Programme for Research and Innovation Leadership in Enabling and Industrial Technologies. Carla Zihlmann reports a relationship with Geistlich Pharma AG that includes: employment. Niklaus Stiefel reports a relationship with Geistlich Pharma AG that includes: employment.

## Acknowledgments

The project leading to this application has received funding from the European Union's Horizon 2020 research and innovation programme under grant agreement No 814444 (MEFISTO). The authors thank Mariarosaria Bonetti and Roberta Marzella for technical and project management support, respectively. Geistlich Pharma AG is kindly acknowledged for providing the medical grade collagen.

## Appendix A. Supplementary data

Supplementary data to this article can be found online at https://doi.org/10.1016/j.heliyon.2023.e23107.

## References


[1] D. Shriram, G. Praveen Kumar, F. Cui, Y.H.D. Lee, K. Subburaj, Evaluating the effects of material properties of artificial meniscal implant in the human knee joint using finite element analysis, Sci. Rep. 7 (2017) 6011.

[2] E. Stocco, A. Porzionato, E. De Rose, S. Barbon, R. De Caro, V. Macchi, Meniscus regeneration by 3D printing technologies: current advances and future perspectives, J. Tissue Eng. 13 (2022), 20417314211065860.

[3] G. Filardo, M. Petretta, C. Cavallo, L. Roseti, S. Durante, U. Albisinni, B. Grigolo, Patient-specific meniscus prototype based on 3D bioprinting of human cell-laden scaffold, Bone & Joint Research 8 (2019) 101–106.

[4] P. Buma, M.V. Meel, T.G.V. Tienen, R.P.H. Veth, Tissue engineering of the meniscus, in: W.S. Pietrzak (Ed.), Musculoskeletal Tissue Regeneration, Humana Press, Totowa, NJ, 2008, pp. 327–346, https://doi.org/10.1007/978-1-59745-239-7_16.

[5] E. Bulgheroni, A. Grassi, M. Campagnolo, P. Bulgheroni, A. Mudhigere, A. Gobbi, Comparative study of collagen versus synthetic-based meniscal scaffolds in treating meniscal deficiency in young active population, Cartilage 7 (2016) 29–38.

[6] A.J.S. Fox, F. Wanivenhaus, A.J. Burge, R.F. Warren, S.A. Rodeo, The human meniscus: a review of anatomy, function, injury, and advances in treatment: the Meniscus: anatomy, Function, Injury and Treatment, Clin. Anat. 28 (2015) 269–287, https://doi.org/10.1002/ca.22456.

[7] M.M. Pillai, J. Gopinathan, R. Selvakumar, A. Bhattacharyya, Human knee meniscus regeneration strategies: a review on recent advances, Curr. Osteoporos. Rep. 16 (2018) 224–235, https://doi.org/10.1007/s11914-018-0436-x.

[8] H. Li, P. Li, Z. Yang, C. Gao, L. Fu, Z. Liao, T. Zhao, F. Cao, W. Chen, Y. Peng, Z. Yuan, X. Sui, S. Liu, Q. Guo, Meniscal regenerative scaffolds based on biopolymers and polymers: recent status and applications, Front. Cell Dev. Biol. 9 (2021), 661802, https://doi.org/10.3389/fcell.2021.661802.

[9] B.P. McKeon, K.R. Zaslav, R.H. Alfred, R.M. Alley, R.H. Edelson, W.K. Gersoff, J.E. Greenleaf, C.C. Kaeding, Preliminary results from a US clinical trial of a novel synthetic polymer meniscal implant, Orthopaedic Journal of Sports Medicine 8 (2020), 232596712095241, https://doi.org/10.1177/2325967120952414.

[10] B. Faivre, H. Bouyarmane, G. Lonjon, P. Boisrenoult, N. Pujol, P. Beaufils, Actifit® scaffold implantation: influence of preoperative meniscal extrusion on morphological and clinical outcomes, J. Orthop. Traumatol.: Surgery & Research 101 (2015) 703–708, https://doi.org/10.1016/j.otsr.2015.06.016.

[11] D. Wang, E. Gonzalez-Leon, S.A. Rodeo, K.A. Athanasiou, Clinical replacement strategies for meniscus tissue deficiency, CARTILAGE 13 (2021) 262S–270S, https://doi.org/10.1177/19476035211060512.

[12] B. Bilgen, C.T. Jayasuriya, B.D. Owens, Current concepts in meniscus tissue engineering and repair, Adv. Healthcare Mater. 7 (2018), 1701407, https://doi.org/10.1002/adhm.201701407.

[13] U. D'Amora, A. Ronca, S. Scialla, A. Soriente, P. Manini, J.W. Phua, C. Ottenheim, A. Pezzella, G. Calabrese, M.G. Raucci, L. Ambrosio, Bioactive composite methacrylated gellan gum for 3D-printed bone tissue-engineered scaffolds, Nanomaterials 13 (2023) 772.

[14] U. D'Amora, A. Soriente, A. Ronca, S. Scialla, M. Perrella, P. Manini, J.W. Phua, C. Ottenheim, R. Di Girolamo, A. Pezzella, L. Ambrosio, Eumelanin from the black soldier fly as sustainable biomaterial: characterisation and functional benefits in tissue-engineered composite scaffolds, Biomedicines 10 (2022) 2945.

[15] E. Kon, G. Filardo, M. Tschon, M. Fini, G. Giavaresi, L.M. Reggiani, C. Chiari, S. Nehrer, I. Martin, D.M. Salter, L. Ambrosio, M. Marcacci, Tissue engineering for total meniscal substitution: animal study in sheep model—results at 12 months, Tissue Eng. 18 (2012) 1573–1582, https://doi.org/10.1089/ten.tea.2011.0572.

[16] A. Ronca, U. D'Amora, M.G. Raucci, H. Lin, Y. Fan, X. Zhang, L. Ambrosio, A combined approach of double network hydrogel and nanocomposites based on hyaluronic acid and poly (ethylene glycol) diacrylate blend, Materials 11 (2018) 2454.

[17] U. D'Amora, A. Ronca, M.G. Raucci, H. Lin, A. Soriente, Y. Fan, X. Zhang, L. Ambrosio, Bioactive composites based on double network approach with tailored mechanical, physico-chemical, and biological features, J. Biomed. Mater. Res. 106 (2018) 3079–3089.

[18] U. D'Amora, A. Ronca, M. Raucci, S. Dozio, H. Lin, Y. Fan, X. Zhang, L. Ambrosio, In situ sol-gel synthesis of hyaluronan derivatives bio-nanocomposite hydrogels, Regenerative Biomaterials 6 (2019) 249–258.

[19] L. Ferroni, C. Gardin, U. D'Amora, L. Calzà, A. Ronca, E. Tremoli, L. Ambrosio, B. Zavan, Exosomes of mesenchymal stem cells delivered from methacrylated hyaluronic acid patch improve the regenerative properties of endothelial and dermal cells, Biomater. Adv. 139 (2022), 213000, https://doi.org/10.1016/j.bioadv.2022.213000.

[20] R.C. Advincula, J.R.C. Dizon, E.B. Caldona, R.A. Viers, F.D.C. Siacor, R.D. Maalihan, A.H. Espera, On the progress of 3D-printed hydrogels for tissue engineering, MRS Communications 11 (2021) 539–553.

[21] J.M. Lee, S.K.Q. Suen, W.L. Ng, W.C. Ma, W.Y. Yeong, Bioprinting of collagen: considerations, potentials, and applications, Macromol. Biosci. 21 (2021), 2000280.

[22] S. Ghosh, B. Sarkar, R. Mishra, N. Thorat, S. Thongmee, Collagen Based 3D Printed Scaffolds for Tissue Engineering, 2022.

[23] H. Yoon, J.-S. Lee, H. Yim, G. Kim, W. Chun, Development of cell-laden 3D scaffolds for efficient engineered skin substitutes by collagen gelation, RSC Adv. 6 (2016) 21439–21447, https://doi.org/10.1039/C5RA19532B.

[24] E.O. Osidak, E.P. Kalabusheva, E.V. Alpeeva, S.I. Belousov, S.V. Krasheninnikov, T.E. Grigoriev, S.P. Domogatsky, E.A. Vorotelyak, E.S. Chermnykh, Concentrated collagen hydrogels: a new approach for developing artificial tissues, Materialia 20 (2021), 101217, https://doi.org/10.1016/j.mtla.2021.101217.

[25] E.O. Osidak, P.A. Karalkin, M.S. Osidak, V.A. Parfenov, D.E. Sivogrivov, F.D.A.S. Pereira, A.A. Gryadunova, E.V. Koudan, Y.D. Khesuani, V.A. Kasyanov, Viscoll collagen solution as a novel bioink for direct 3D bioprinting, J. Mater. Sci. Mater. Med. 30 (2019) 1–12.

[26] N. Diamantides, L. Wang, T. Pruiksma, J. Siemiatkoski, C. Dugopolski, S. Shortkroff, S. Kennedy, L.J. Bonassar, Correlating rheological properties and printability of collagen bioinks: the effects of riboflavin photocrosslinking and pH, Biofabrication 9 (2017), 34102.

[27] E. Olegovich Osidak, V. Igorevich Kozhukhov, M. Sergeevna Osidak, S. Petrovich Domogatskiy, Collagen as bioink for bioprinting: a comprehensive review, Int J Bioprint 6 (2020), https://doi.org/10.18063/ijb.v6i3.270.

[28] A. Lode, M. Meyer, S. Brüggemeier, B. Paul, H. Baltzer, M. Schröpfer, C. Winkelmann, F. Sonntag, M. Gelinsky, Additive manufacturing of collagen scaffolds by three-dimensional plotting of highly viscous dispersions, Biofabrication 8 (2016), 015015.

[29] F. Achatz, R. Kujat, C. Pfeifer, M. Koch, M. Nerlich, P. Angele, J. Zellner, In vitro testing of scaffolds for mesenchymal stem cell-based meniscus tissue engineering—introducing a new biocompatibility scoring system, Materials 9 (2016) 276, https://doi.org/10.3390/ma9040276.

[30] G. Pattappa, R. Schewior, I. Hofmeister, J. Seja, J. Zellner, B. Johnstone, D. Docheva, P. Angele, Physioxia has a beneficial effect on cartilage matrix production in interleukin-1 beta-inhibited mesenchymal stem cell chondrogenesis, Cells 8 (2019) 936, https://doi.org/10.3390/cells8080936.

[31] G. Pattappa, F. Reischl, J. Jahns, R. Schewior, S. Lang, J. Zellner, B. Johnstone, D. Docheva, P. Angele, Fibronectin adherent cell populations derived from avascular and vascular regions of the meniscus have enhanced clonogenicity and differentiation potential under physioxia, Front. Bioeng. Biotechnol. 9 (2022), 789621.

[32] X. Yang, Z. Lu, H. Wu, W. Li, L. Zheng, J. Zhao, Collagen-alginate as bioink for three-dimensional (3D) cell printing based cartilage tissue engineering, Mater. Sci. Eng. C 83 (2018) 195–201.

[33] W. Kim, C.H. Jang, G. Kim, Optimally designed collagen/polycaprolactone biocomposites supplemented with controlled release of HA/TCP/rhBMP-2 and HA/TCP/PRP for hard tissue regeneration, Mater. Sci. Eng. C 78 (2017) 763–772, https://doi.org/10.1016/j.msec.2017.04.144.

[34] Y. Song, S. Hua, S. Sayyar, Z. Chen, J. Chung, X. Liu, Z. Yue, C. Angus, B. Filippi, S. Beirne, G. Wallace, G. Sutton, J. You, Corneal bioprinting using a high concentration pure collagen I transparent bioink, Bioprinting 28 (2022), e00235, https://doi.org/10.1016/j.bprint.2022.e00235.

[35] J.H.Y. Chung, S. Naficy, Z. Yue, R. Kapsa, A. Quigley, S.E. Moulton, G.G. Wallace, Bio-ink properties and printability for extrusion printing living cells, Biomater. Sci. 1 (2013) 763–773.

[36] D.L. Cohen, W. Lo, A. Tsavaris, D. Peng, H. Lipson, L.J. Bonassar, Increased mixing improves hydrogel homogeneity and quality of three-dimensional printed constructs, Tissue Eng. C Methods 17 (2011) 239–248.

[37] J. Lee, S.J. Oh, S.H. An, W.-D. Kim, S.-H. Kim, Machine learning-based design strategy for 3D printable bioink: elastic modulus and yield stress determine printability, Biofabrication 12 (2020), 035018, https://doi.org/10.1088/1758-5090/ab8707.

[38] S.P. Tarassoli, Z.M. Jessop, T. Jovic, K. Hawkins, I.S. Whitaker, Candidate bioinks for extrusion 3D bioprinting—a systematic review of the literature, Front. Bioeng. Biotechnol. 9 (2021), 616753, https://doi.org/10.3389/fbioe.2021.616753.

[39] A. Pössl, D. Hartzke, T.M. Schmidts, F.E. Runkel, P. Schlupp, A targeted rheological bioink development guideline and its systematic correlation with printing behavior, Biofabrication 13 (2021), 035021, https://doi.org/10.1088/1758-5090/abde1e.

[40] M.E. Cooke, D.H. Rosenzweig, The rheology of direct and suspended extrusion bioprinting, APL Bioeng. 5 (2021), 011502.

[41] B.R. Maciel, K. Baki, C. Oelschlaeger, N. Willenbacher, The influence of rheological and wetting properties of hydrogel-based bio-inks on extrusion-based bioprinting, Chem. Ing. Tech. 94 (2022) 393–401, https://doi.org/10.1002/cite.202100139.

[42] D.V. Shepherd, J.H. Shepherd, S. Ghose, S.J. Kew, R.E. Cameron, S.M. Best, The process of EDC-NHS cross-linking of reconstituted collagen fibres increases collagen fibrillar order and alignment, Apl. Mater. 3 (2015), 14902.

[43] E. Afnor, NF EN ISO 11137-1, July 2006. Sterilization of Health Care Products-Irradiation-Part 1: Requirements for Development, Validation and Routine Control of a Sterilization Process for Medical Devices, 2006.

[44] X. Deng, X. Chen, F. Geng, X. Tang, Z. Li, J. Zhang, Y. Wang, F. Wang, N. Zheng, P. Wang, Precision 3D printed meniscus scaffolds to facilitate hMSCs proliferation and chondrogenic differentiation for tissue regeneration, J. Nanobiotechnol. 19 (2021) 1–19.

[45] Z.-Z. Zhang, D. Jiang, J.-X. Ding, S.-J. Wang, L. Zhang, J.-Y. Zhang, Y.-S. Qi, X.-S. Chen, J.-K. Yu, Role of scaffold mean pore size in meniscus regeneration, Acta Biomater. 43 (2016) 314–326, https://doi.org/10.1016/j.actbio.2016.07.050.

[46] A.V. Vasiliadis, N. Koukoulias, K. Katakalos, Three-dimensional-printed scaffolds for meniscus tissue engineering: opportunity for the future in the orthopaedic world, J. Forensic Biomech. 12 (2021) 69, https://doi.org/10.3390/jfb12040069.

[47] J.A. Stammen, S. Williams, D.N. Ku, R.E. Guldberg, Mechanical properties of a novel PVA hydrogel in shear and unconfined compression, Biomaterials 22 (2001) 799–806, https://doi.org/10.1016/S0142-9612(00)00242-8.

[48] M.M. Smoak, A. Han, E. Watson, A. Kishan, K.J. Grande-Allen, E. Cosgriff-Hernandez, A.G. Mikos, Fabrication and characterization of electrospun decellularized muscle-derived scaffolds, Tissue Eng. C Methods 25 (2019) 276–287, https://doi.org/10.1089/ten.tec.2018.0339.

[49] D.E. Anderson, B. Johnstone, Dynamic mechanical compression of chondrocytes for tissue engineering: a critical review, Front. Bioeng. Biotechnol. 5 (2017) 76.

[50] M.A. Geven, A. Lapomarda, O. Guillaume, C.M. Sprecher, D. Eglin, G. Vozzi, D.W. Grijpma, Osteogenic differentiation of hBMSCs on porous photo-crosslinked poly (trimethylene carbonate) and nano-hydroxyapatite composites, Eur. Polym. J. 147 (2021), 110335.

[51] H. Pereira, S.G. Caridade, A.M. Frias, J. Silva-Correia, D.R. Pereira, I.F. Cengiz, J.F. Mano, J.M. Oliveira, J. Espregueira-Mendes, R.L. Reis, Biomechanical and cellular segmental characterization of human meniscus: building the basis for Tissue Engineering therapies, Osteoarthritis Cartilage 22 (2014) 1271–1281, https://doi.org/10.1016/j.joca.2014.07.001.

[52] J. Lee, Md Sultan, S. Kim, V. Kumar, Y. Yeon, O. Lee, C. Park, Artificial auricular cartilage using silk fibroin and polyvinyl alcohol hydrogel, Indian J. Manag. Sci. 18 (2017) 1707, https://doi.org/10.3390/ijms18081707.

[53] S. Xu, X. Li, Y. Wang, Z. Hu, R. Wang, Characterization of slow-release collagen- *g* -poly(acrylic acid- *co* -2-acrylamido-2-methyl-1-propane sulfonic acid)-iron (III) superabsorbent polymer containing fertilizer, J. Appl. Polym. Sci. 136 (2019), 47178, https://doi.org/10.1002/app.47178.

[54] E. Jahed, M.A. Khaledabad, H. Almasi, R. Hasanzadeh, Physicochemical properties of Carum copticum essential oil loaded chitosan films containing organic nanoreinforcements, Carbohydr. Polym. 164 (2017) 325–338.

[55] W.M.G.A.C. Groen, L. Utomo, M. Castilho, D. Gawlitta, J. Malda, P.R.V. Weeren, R. Levato, N.M. Korthagen, Impact of endotoxins in gelatine hydrogels on chondrogenic differentiation and inflammatory cytokine secretion in vitro, Indian J. Manag. Sci. 21 (2020) 8571, https://doi.org/10.3390/ijms21228571.

[56] D. Calder, A. Fathi, F. Oveissi, S. Maleknia, T. Abrams, Y. Wang, J. Maitz, K.H. Tsai, P. Maitz, W. Chrzanowski, I. Canoy, V.A. Menon, K. Lee, B.J. Ahern, N. E. Lean, D.M. Silva, P.M. Young, D. Traini, H.X. Ong, R.S. Mahmoud, H. Montazerian, A. Khademhosseini, F. Dehghani, Thermoresponsive and injectable hydrogel for tissue agnostic regeneration, Adv. Healthcare Mater. 11 (2022), 2201714, https://doi.org/10.1002/adhm.202201714.

[57] E.A. Makris, P. Hadidi, K.A. Athanasiou, The knee meniscus: structure–function, pathophysiology, current repair techniques, and prospects for regeneration, Biomaterials 32 (2011) 7411–7431.

[58] C.A. Mcdevitt, R.J. Webber, The ultrastructure and biochemistry of meniscal cartilage, Clin. Orthop. Relat. Res. 252 (1990) 8–18.

[59] B. Andress, J.H. Kim, H.C. Cutcliffe, A. Amendola, A.P. Goode, S. Varghese, L.E. DeFrate, A.L. McNulty, Meniscus cell regional phenotypes: dedifferentiation and reversal by biomaterial embedding, J. Orthop. Res. 39 (2021) 2177–2186, https://doi.org/10.1002/jor.24954.

[60] J. Chahla, A. Papalamprou, V. Chan, Y. Arabi, K. Salehi, T.J. Nelson, O. Limpisvasti, B.R. Mandelbaum, W. Tawackoli, M.F. Metzger, Assessing the resident progenitor cell population and the vascularity of the adult human meniscus, Arthrosc. J. Arthrosc. Relat. Surg. 37 (2021) 252–265.

[61] B.D. Andress, R.M. Irwin, I. Puranam, B.D. Hoffman, A.L. McNulty, A tale of two loads: modulation of IL-1 induced inflammatory responses of meniscal cells in two models of dynamic physiologic loading, Front. Bioeng. Biotechnol. 10 (2022), 837619, https://doi.org/10.3389/fbioe.2022.837619.

[62] A.R.A. Szojka, D.X. Li, M.E.J. Sopcak, Z. Ma, M. Kunze, A. Mulet-Sierra, S.M. Adeeb, L. Westover, N.M. Jomha, A.B. Adesida, Mechano-hypoxia conditioning of engineered human meniscus, Front. Bioeng. Biotechnol. 9 (2021), 739438, https://doi.org/10.3389/fbioe.2021.739438.

[63] L. Bacakova, J. Pajorova, M. Bacakova, A. Skogberg, P. Kallio, K. Kolarova, V. Svorcik, Versatile application of nanocellulose: from industry to skin tissue engineering and wound healing, Nanomaterials 9 (2019) 164.

[64] M. Raimondi, L. Falcone, M. Colombo, A. Remuzzi, E. Marinoni, M. Marazzi, V. Rapisarda, R. Pietrabissa, A comparative evaluation of chondrocyte/scaffold constructs for cartilage tissue engineering, J. Appl. Biomater. Biomech. 2 (2004) 55–64.

[65] Y. Zhang, S.T. Ellison, S. Duraivel, C.D. Morley, C.R. Taylor, T.E. Angelini, 3D printed collagen structures at low concentrations supported by jammed microgels, Bioprinting 21 (2021), e00121.

[66] C.C. Clark, J. Aleman, L. Mutkus, A. Skardal, A mechanically robust thixotropic collagen and hyaluronic acid bioink supplemented with gelatin nanoparticles, Bioprinting 16 (2019), e00058.

[67] E. Sachlos, N. Reis, C. Ainsley, B. Derby, J. Czernuszka, Novel collagen scaffolds with predefined internal morphology made by solid freeform fabrication, Biomaterials 24 (2003) 1487–1497.

[68] W. Yeong, C. Chua, K. Leong, M. Chandrasekaran, M. Lee, Comparison of drying methods in the fabrication of collagen scaffold via indirect rapid prototyping, J. Biomed. Mater. Res. B Appl. Biomater. 82 (2007) 260–266.